



HAL
open science

A cyclogenesis evolving into two distinct scenarios and its implications for short-term ensemble forecasting

Matthieu Plu, Philippe Arbogast

► **To cite this version:**

Matthieu Plu, Philippe Arbogast. A cyclogenesis evolving into two distinct scenarios and its implications for short-term ensemble forecasting. *Monthly Weather Review*, 2005, 133 (7), pp.2016–2029. 10.1175/MWR2955.1 . meteo-00195293

HAL Id: meteo-00195293

<https://meteofrance.hal.science/meteo-00195293>

Submitted on 12 Feb 2021

HAL is a multi-disciplinary open access archive for the deposit and dissemination of scientific research documents, whether they are published or not. The documents may come from teaching and research institutions in France or abroad, or from public or private research centers.

L'archive ouverte pluridisciplinaire **HAL**, est destinée au dépôt et à la diffusion de documents scientifiques de niveau recherche, publiés ou non, émanant des établissements d'enseignement et de recherche français ou étrangers, des laboratoires publics ou privés.

A Cyclogenesis Evolving into Two Distinct Scenarios and Its Implications for Short-Term Ensemble Forecasting

MATTHIEU PLU AND PHILIPPE ARBOGAST

CNRM/GMAP/RECYF, Météo-France, Toulouse, France

(Manuscript received 6 April 2004, in final form 16 December 2004)

ABSTRACT

In a nonlinear quasigeostrophic model with uniform potential vorticity, an idealized initial state sharing some features with atmospheric low-predictability situations is built. Inspired by previous work on idealized cyclogenesis, two different cyclogenesis scenarios are obtained as a result of a small change of the initial location of one structure. This behavior is interpreted by analyzing the baroclinic interaction between upper- and lower-level anomalies. The error growth mechanism is nonlinear; it does not depend on the linear stability properties of the jet, which are the same in both evolutions.

The ability of ensemble forecasts to capture these two possible evolutions is then assessed given some realistic error bounds in the knowledge of the initial conditions. First, a reference statistical distribution of each of the evolutions is obtained by means of a large Monte Carlo ensemble. Smaller ensembles with size representative of what is available in current operational implementations are then built and compared to the Monte Carlo reference: several singular-vector-based ensembles, a small Monte Carlo ensemble, and a “coherent structure”-based ensemble. This new technique relies on a sampling of the errors on the precursors of the cyclogenesis: amplitude and position errors. In this context, the precursors are handled as coherent structures that may be amplified or moved within realistic error bounds. It is shown that the singular vector ensemble fails to reproduce the bimodal distribution of the variability if the ensemble is not initially constrained, whereas it is accessible at a relatively low cost to the new coherent structures initialization.

1. Introduction

The predictability of cyclogenesis is an essential issue in order to improve the forecast of midlatitude extreme events. The experience of recent strong storms in Europe and some studies (Hoskins and Berrisford 1988; Hello and Arbogast 2004) show that the deterministic forecast of storms by numerical models may fail, even for terms as short as 24 h and particularly for the most severe ones. Forecast errors have two causes. First, the numerical model is an imperfect representation of the atmospheric governing laws: approximations and physical parameterizations create or amplify a deviation from the real state of the atmosphere (model errors). Second, the atmospheric system and the model are chaotic in some regimes. In these flows, Lorenz (1963)

showed that there is a strong dependence on the initial state. As far as midlatitude cyclones are concerned, the nonlinear phenomena that occur during their development (Simmons and Hoskins 1978; Thorncroft and Hoskins 1990; Mullen and Baumhefner 1994) may generate flows for which the predictability is weak. Since the true initial state is impossible to define as accurately as needed, small errors at the initial time may yield a huge discrepancy some time later (initial condition error). For these flows the deterministic simulation may just be one possible scenario among all the evolutions obtained by slightly changing the initial conditions. As for medium-range forecasts, ensemble forecasting may be a practical efficient alternative to deterministic forecasting, but the extension of the method to short-term forecasting may not be straightforward. In particular, the strategy for building the initial perturbations has to be examined. The present study assumes that the model is perfect (Hamill et al. 2000) and concentrates on the dependence on initial conditions for the development of a cyclone.

Corresponding author address: Matthieu Plu, Météo-France, CNRM/GMAP/RECYF, 42 avenue G. Coriolis, 31057 Toulouse Cedex, France.
E-mail: matthieu.plu@meteo.fr

The aim of ensemble forecasting (Molteni et al. 1996) is to approximate the probability density function (PDF) of the atmospheric state. In a perfect-model framework, the emphasis is put on the choice of an appropriate perturbation method. Leith (1974) proposed the Monte Carlo method, which consists of a random sampling of the initial PDF. This ensemble approximates the propagation of the PDF by the model with a good accuracy provided it is large enough, but then it is far too expensive to be used operationally. Other ensemble techniques aim at doing the same with a reasonable numerical cost, following different strategies.

The National Centers for Environmental Prediction (NCEP) bred modes (Toth and Kalnay 1993) are the optimal perturbations that have grown the most rapidly before the initial instant. They are usually taken as a fair method to sample the PDF of the analysis error, requiring an assimilation cycle. The European Centre for Medium-Range Weather Forecasts (ECMWF) singular vectors (Molteni et al. 1996) are the modes that maximize the linear growth of energy over a specified domain. They may be constrained by an estimate of the analysis error PDF (Barkmeijer et al. 1999) by changing the initial norm for the computation of the singular vectors (Ehrendorfer and Tribbia 1997). Recently, Ziehmann (2000) and Richardson (2001) proposed multianalyses and multimodel ensembles, which give encouraging operational results. These are efficient ways to both sample the analysis error and simulate the model error.

The present paper concentrates on the methods that are constrained by the dynamics of the model, that is, mainly singular vectors. The analysis error is unknown; no observations are available and no assimilation cycle may be computed. In this framework a good ensemble is supposed to approach the intrinsic variability of the dynamical system.

The use of singular vectors as a condensed way to represent the PDF of the atmospheric state relies on a linear assumption: the errors that may grow the most rapidly soon after the initial instant are the singular modes of the tangent-linear model. However in some idealized flows, Snyder (1999) showed mechanisms of error growth that are not linked to linear instabilities. An initial error in the phase of a wave or in the position or amplitude of a coherent structure may grow nonlinearly by interaction with the medium of propagation or other finite-amplitude structures. For these flows for which the error growth mechanism is not linked to linear instability, the validity of singular vectors as optimal initial perturbations may not be clear. This may be particularly true for the short-term forecast of a deep cy-

clone because of the local nonlinear interactions that are possibly involved [such a cyclogenesis is presented in Arbogast (2004)]. Is the error growth mechanism crucial to determining the most relevant initial perturbations? This issue will be addressed further in the paper.

The purpose of this paper is to build a particular flow, sharing features with low-predictability weather cases in an idealized meteorological model and to assess the benefits of ensemble prediction settings. The quasigeostrophic model with uniform potential vorticity that is used is nonlinear. The initial state is entirely controlled, as it is an idealized cyclone defined by a limited number of parameters (position, amplitude, and orientation). Although the nonlinear terms are fewer and weaker than in an operational model, distinct scenarios of evolution can be obtained sharing features of a low-predictability situation in a chaotic system. The low numerical cost of this model and its small number of degrees of freedom ($\approx 10^4$) allow the computation of a large reference Monte Carlo ensemble. The initial PDF of this ensemble follows some kind of climatological error of the dynamic model. Three singular vector ensembles are computed and they are compared to the reference ensemble. Two ensembles of various sizes obtained by slight modifications of the initial structure of the cyclone are calculated and assessed. Section 2 reviews the quasigeostrophic assumptions and equations. The definition of the idealized initial cyclones is also developed. In section 3, a low-predictability initial state is shown for which a physical interpretation is given. Section 4 describes the results from different ensemble prediction systems, which are initialized successively by singular vectors, Monte Carlo technique, or the variation of the parameters that define the initial cyclone. Finally, section 5 is devoted to the link between the error growth mechanism and the initial sampling of an ensemble.

2. Experimental framework

a. The model

The theory of the quasigeostrophic model with uniform potential vorticity is reviewed here. The troposphere is represented by an adiabatic, inviscid, and incompressible fluid in a three-dimensional domain. The horizontal domain is an f -plane channel with periodic boundary conditions in both x and y . The vertical coordinate z is defined as the pseudoheight of Hoskins and Bretherton (1972) and is bounded by lower and upper rigid lids. The primitive equations are filtered so that the terms with high Rossby number are discarded. The geopotential $\Phi(x, y, z, t)$ and the potential tem-

perature $\theta(x, y, z, t)$ are the prognostic fields of the balanced flow. They are divided in the sum of a known constant basic state (Φ_b, θ_b) and a perturbation (Φ', θ') .

The following assumptions are made:

- a low Rossby number $R_0 = U(fL)^{-1} \ll 1$;
- the Coriolis parameter f is uniform ($f = 10^{-4} \text{ s}^{-1}$);
- the Boussinesq approximation: the pseudodensity does not depend on z ;
- the basic state is a function of z and the Brunt–Väisälä frequency $N = (g\theta_0^{-1}\partial\theta_b/\partial z)^{1/2}$ is uniform. Therefore the basic-state stratification can be written as $\theta_b(z) = \theta_0(1 + N^2g^{-1}z)$.

From the quasigeostrophic equations, it follows that the quasigeostrophic potential vorticity

$$q_g = f + f^{-1}\nabla^2\Phi' + \frac{\partial}{\partial z}\left(fN^{-2}\frac{\partial\Phi'}{\partial z}\right) \quad (1)$$

is a Lagrangian invariant with respect to the horizontal geostrophic velocity. It is then supposed that q_g is uniform in the troposphere and remains so.

The ' symbol on the perturbation fields is deleted from now on, and the equations to be applied in the three-dimensional domain are recalled:

$$\nabla^2\Phi + (f^2N^{-2})\frac{\partial^2\Phi}{\partial z^2} = 0, \quad (2)$$

$$\nabla\Phi = f\mathbf{k} \times \mathbf{u}_g, \quad (3)$$

$$\frac{\partial\Phi}{\partial z} = g\theta_0^{-1}\theta, \quad (4)$$

where \mathbf{u}_g is the geostrophic wind velocity. On the upper and lower boundaries the vertical velocity $w = 0$, thus

$$\left(\frac{\partial}{\partial t} + \mathbf{u}_g \cdot \nabla\right)\theta = 0. \quad (5)$$

The state vector consists of the potential temperature at the lower (ground) level θ^- and at the upper (tropopause) level θ^+ , and both are decomposed in a Fourier basis:

$$\theta^\pm(x, y) = \sum_{m,n=-\infty}^{+\infty} \hat{\theta}_{m,n}^\pm \exp(2\pi imxL_x^{-1}) \exp(2\pi inyL_y^{-1}). \quad (6)$$

A classical elliptic truncation is defined such that the resolution of the collocation grid is 100 km in both dimensions, which is adapted to the synoptic-scale dynamic.

All the other fields in three dimensions (geopotential, relative vorticity, geostrophic wind velocity, and vertical velocity) may be derived from the potential

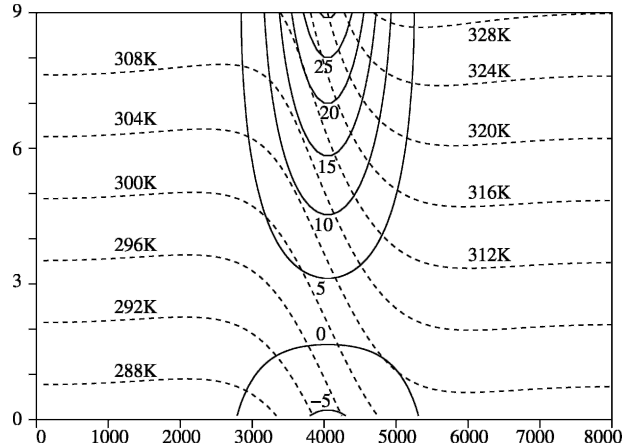


FIG. 1. Vertical cross section across the jet showing isentropes (dashed lines, unity: K) and isotachs (solid lines, unity: m s^{-1}). Dimensions of the domain: $8000 \text{ km} \times 9 \text{ km}$.

temperature through the quasigeostrophic equations. The computation of vertical velocity w is particularly nontrivial as it is obtained through the omega equation

$$\left(N^2\nabla^2 + f^2\frac{\partial^2}{\partial z^2}\right)w = \frac{\partial}{\partial z}[\mathbf{u}_g \cdot \nabla(\nabla^2\Phi)] - g\theta_0^{-1}\nabla^2(\mathbf{u}_g \cdot \nabla\theta). \quad (7)$$

The symmetric baroclinic jet stream is the same as the one described in Davies et al. (1991). Figure 1 reproduces the isentropes and the wind speed of this jet stream, which is a steady state of the quasigeostrophic system. The horizontal coordinate vectors are defined such that y is oriented along the jet and x points toward the warm air. The Fourier transform requires that the θ^\pm fields for the jet are periodic, which is actually not the case in the x direction. Periodicity is obtained by subtracting the linear function of x joining $\theta(x=0, y)$ and $\theta(x=L_x, y)$ and treating it as a linear term in Eq. (5). Indeed the derivative of θ is periodic too, which guarantees that the relative vorticity may be calculated precisely. Table 1 presents the parameters of the model.

TABLE 1. Parameters and numerical values.

Horizontal dimensions of the domain	L_x, L_y	8000 km, 16 000 km
Elliptic truncation wavenumbers	M_f, N_f	40, 80
Troposphere width	H	9 km
Maximal wind speed of the jet stream	V_{\max}	30 m s^{-1}
Coriolis parameter	f	10^{-4} s^{-1}
Brunt–Väisälä frequency	N	10^{-2} s^{-1}
Surface potential temperature of the basic state	θ_0	286 K
Size of the Monte Carlo ensemble	n_{MC}	2000

b. A cyclone model

On top of the jet stream, anomalies of potential temperature are added initially. Each anomaly has the following form (inspired by Schär and Wernli 1993):

$$\theta(x, y) = \theta_M \times \left[h(x, y) - \frac{1}{2} h(x, y - y_s) - \frac{1}{2} h(x, y + y_s) \right], \quad (8)$$

with $h(x, y) = \{1 + [(x - x_0) \cos\phi + (y - y_0) \sin\phi]^2 a^{-2} + [-(x - x_0) \sin\phi + (y - y_0) \cos\phi]^2 b^{-2}\}^{-3/2}$. Therefore, an anomaly is composed of three ellipses aligned parallel to the jet and regularly spaced by y_s . Here (x_0, y_0) is the center of the central ellipse, a and b the length of its axes, ϕ the angle between its major axis and the jet, and θ_M the amplitude of the anomaly. If this localized anomaly is far enough from the boundaries of the horizontal domain, the periodicity of the θ field is ensured. This tripolar structure of potential temperature gives no contribution to the sum $\iint_S \theta \, dS$. In addition, as explained by Schär and Wernli (1993), it also excites shorter wavelengths than a monopolar structure.

An idealized cyclone consists initially of two anomalies, one at the tropopause and the other at the surface. Twelve independent parameters describe the initial cyclone: $\theta_M, x_0, a, b, \phi$, for each anomaly, plus y_s and the distance along the jet between the two anomalies $y_0^+ - y_0^-$. From this, instead of using the parameters a, b , the eccentricity and the length of the major axis of the ellipse will be the relevant parameters to characterize the ellipse. The parameter $d = y_0^+ - y_0^-$ will be called *vertical tilt*.

The amplitude of an anomaly is defined by θ_M . Since in a quasigeostrophic model with uniform potential vorticity the two levels play a symmetric role, both anomalies may be defined in the same manner. In an operational model one should be careful that an upper anomaly has a larger amplitude in order to give the same impact on a cyclone.

It is expected that the interaction between the upper and the lower anomalies superposed upon a baroclinic zone depends on their features, which means also that the cyclogenesis would depend on the 12 initial parameters. Finding a low-predictability situation according to this definition of an initial state is the purpose of the following section.

3. A low-predictability situation

To find an initial state with low predictability, the space of initial parameters has been explored. A par-

ticular initial state mentioned by Schär and Wernli (1993) emerged as having some characteristics of a low-predictability situation. Suppose one has selected a configuration of the initial parameters for which the cyclogenesis is explosive. For these initial parameters, the interaction between both anomalies is strong, which creates a single intense surface cyclone. Changing the initial vertical tilt has a large impact on the final state. If this parameter increases too much, then the baroclinic interaction between the upper and lower anomalies is lost. So a transition is expected from baroclinic interaction to noninteraction as the vertical tilt increases, and this transition may be rapid.

The *control initial state* \mathbf{X}_0 is selected as a state for which a surface cyclone evolves and deepens fast. The whole simulation starting from \mathbf{X}_0 is called *control*. Its initial vertical tilt is such that baroclinic interaction exists, but is not optimal for it. Let \mathbf{X}'_0 be the secondary initial state, which is obtained by increasing the vertical tilt of \mathbf{X}_0 by 100 km. The simulation starting from \mathbf{X}'_0 is the *secondary scenario*.

A main cyclonic vortex MV is present in both evolutions and the secondary scenario is distinguished by two vortices located upstream of MV: a cyclonic zone C and an anticyclonic core Ac. The simulations last 96 h, which is considered as the final time of the forecast. Maps of relative vorticity at the ground level are computed and shown in Fig. 2. The region of Ac at the final time is called \mathfrak{R} . It is important to notice that the low-predictability situation is local, which is relevant for short-term forecasting.

A more comprehensive dynamical interpretation is proposed. Figure 3 shows the maps of relative vorticity at the surface for both scenarios at 24 and 48 h. The different features between the two scenarios are obvious starting from 48 h and are maintained through 96 h. The physical cause of the two distinct scenarios just before 48 h may be understood by looking at the vertical velocity associated with the upper-level field (Fig. 4). This vertical velocity field is obtained by solving Eq. (7) with the potential temperature of the perturbation set to 0 at the lower level. In quasigeostrophic systems a significant source of relative vorticity is the stretching effect entailed by vertical velocity. This nonlinear effect is a sign of the baroclinic interaction between coherent structures. In the secondary scenario, one core A of negative vertical velocity (downward) is stronger than in the control scenario and one core B of positive vertical velocity (upward) has appeared. The positions of these cores can be associated with the vorticity structures on the ground: A is associated with Ac and B with MV. These associations are consistent with the quasi-

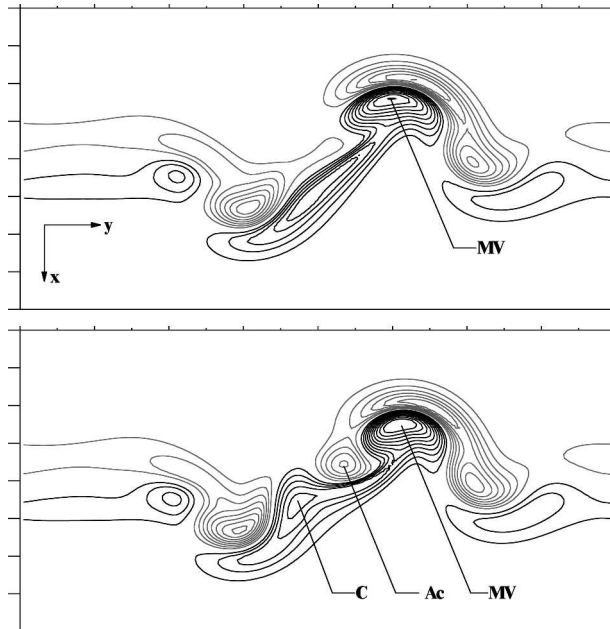


FIG. 2. Relative vorticity at the ground level at time 96 h. Black contours are positive vorticity, and gray contours are negative. Intervals: $5 \times 10^{-6} \text{ s}^{-1}$. The size of the domain is $16\,000 \text{ km} \times 8000 \text{ km}$. The jet stream goes from left to right. (top) Control run **X**. (bottom) Secondary scenario **X'**. The main cyclonic vortex MV exists in both scenarios. The secondary scenario has two vortices in addition to the control, one anticyclonic Ac and one cyclonic C. The region \mathfrak{R} is the one around the Ac vortex.

geostrophic theory: upward movement generates cyclonic vorticity and downward movement generates anticyclonic vorticity.

So the structure Ac is created by baroclinic interac-

tion, and the wind thus generated makes the cyclone C appear. The anticyclone Ac is very specific of the secondary scenario; this is why this work will further concentrate on this structure and on the region \mathfrak{R} . Thus, it is demonstrated that the low predictability of the flow is due to the loss of baroclinic interaction between the upper- and lower-level structures. This interaction between lower- and upper-level structures was extensively studied by Takayabu (1991). In a more complex model where the humidity variable is taken into account and a convective parameterization scheme implemented, the positive vertical velocity would be reinforced by nonlinear processes and the separation between the two scenarios would likely be more dramatic.

The two scenarios are also distinguishable in terms of potential temperature. Initially, the maximum difference of potential temperature between the two states is 0.8 K. At the end of the forecast (96 h), it becomes 8 K. The spread has rapidly increased in 96 h.

A 96-h forecast is not a short-term prediction for operational meteorology. This time of integration relies on the fact that the evolution of the quasigeostrophic cyclone is slow: the nonlinearities in this model are not as intense as in the real atmosphere or in an operational model. In particular, the dry atmosphere assumption slows the cyclone growth. As stated by Thorncroft and Hoskins (1990), the implementation of a convection scheme would decrease drastically the effective Brunt-Väisälä frequency N . The growth rate $\chi \propto fN^{-1}$ of Eady linear normal modes would increase and the cyclone would deepen significantly faster. Emanuel et al. (1987) obtained a growth rate 2.6 times larger by using a

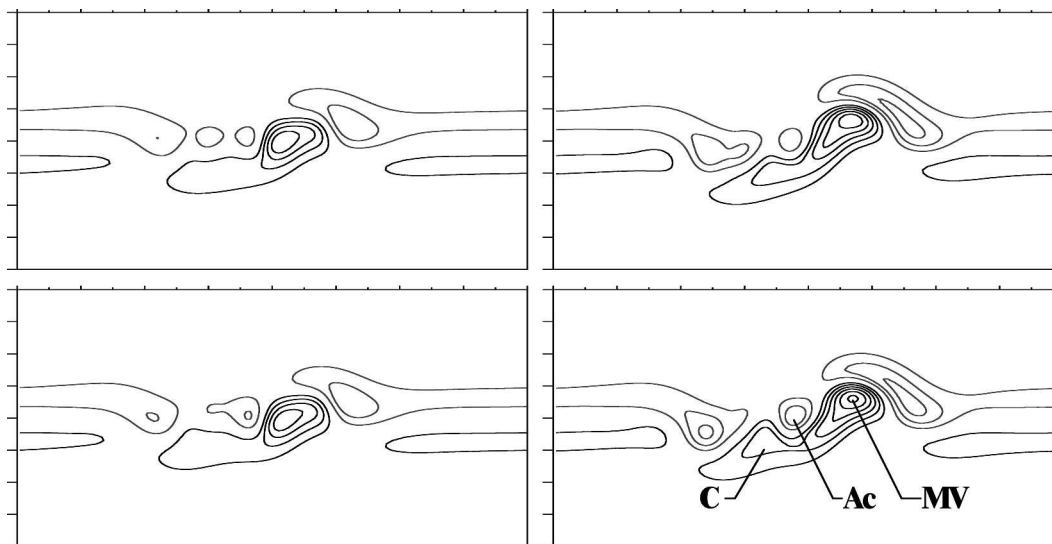


FIG. 3. Relative vorticity at the ground level at time (left) 24 and (right) 48 h for the (top) control scenario **X** and (bottom) secondary scenario **X'**. Same contours as in Fig. 2. The three structures MV, Ac, and C may be recognized from Fig. 2, although they are weaker at 48 h than at 96 h.

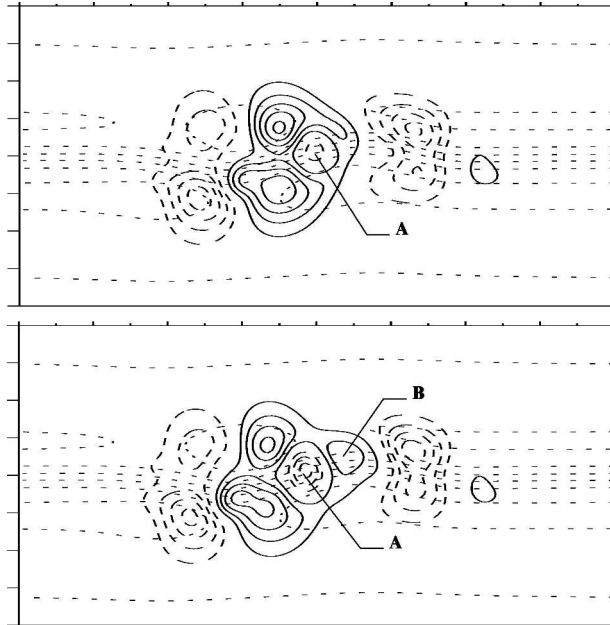


FIG. 4. Vertical velocity at altitude 4.5 km (midlevel) at time 24 h created by the upper anomalies. Plain contours are positive velocity (upward movement), and dashed contours are negative velocity (downward movement). Intervals: $2 \times 10^{-3} \text{ m s}^{-1}$. The dotted contours show the potential temperature field at the upper level (tropopause). Intervals: 3 K. (top) The control scenario and (bottom) the secondary scenario. In the secondary scenario the negative vertical velocity core A is stronger and a positive velocity core B appears. Through stretching on the lower level, A makes the anticyclonic core Ac appear in the secondary scenario and B strengthens the main cyclone MV (see Fig. 3).

simple scheme. A 96-h term was chosen because it lets the cyclone strengthen enough.

4. Ensemble prediction around this initial state

The control initial state leads to a flow with low-predictability properties, and different kinds of ensembles are built around this initial state. A Monte Carlo ensemble will be built for reference: it will be as large as required to derive stable statistics from it. This ensemble will be used for comparison with small ensembles whose size will be representative of an operational ensemble forecast.

a. Construction of the ensembles

An ensemble is a condensed way to represent the PDF of the atmospheric state (Molteni et al. 1996). Each ensemble explores various directions in the phase space and has a given variance. As the purpose of this work is to assess different strategies for building ensembles, it is necessary to make sure that all the en-

sembles that are defined have initially the same variance, which depends on the climatological analysis error. The procedure used to define each initial ensemble follows. Let n be the size of an ensemble. The potential temperature of each initial state in the ensemble is decomposed as the sum of the control initial state and a perturbation:

$$\theta_i^+ = \theta_c^+ + \theta_i'^+, \tag{9}$$

$$\theta_i^- = \theta_c^- + \theta_i'^- \quad \forall i = 1 \dots n, \tag{10}$$

where + and - refer, respectively, to the upper and lower level of the model, θ_c is the potential temperature of the control state, and θ_i' is the perturbation of the i th member of the ensemble.

At every grid point belonging to any of the two levels, the *spread* (square root of variance) of θ in the ensemble is defined as

$$\sigma_\theta(x, y) = \{(n - 1)^{-1} \sum_{i=1}^n [\theta_i(x, y) - \bar{\theta}(x, y)]^2\}^{1/2}, \tag{11}$$

where classically $\bar{\theta}(x, y)$ is the mean of potential temperature of the ensemble at the point (x, y) .

The amplitude of the perturbations of any ensemble has to be consistent with the uncertainty on the initial state. They are normalized initially and the maximum spread of potential temperature equals the climatological analysis error $\sigma_0 = 0.6 \text{ K}$ in the midlatitudes of the Northern Hemisphere, so that

$$\max_{(x, y)} [\sigma_{\theta^+}(x, y), \sigma_{\theta^-}(x, y)] = \sigma_0.$$

In the quasigeostrophic model the upper and the lower levels play a symmetric role, which explains why σ_0 is the same for both levels. In a more complex setting, σ_0 should vary with altitude.

b. Methods to assess the ensembles

A large Monte Carlo ensemble is built. Its ability to represent the variability of the dynamical system and to be taken as a reference is discussed now.

Leith (1974) assessed the capability of the Monte Carlo ensemble to represent the stochastic distribution of the true state of the atmosphere. The Monte Carlo ensemble is a cloud of random possible states that propagates with time in the phase space. At the final time of the simulation all directions have been explored and the resulting ensemble represents the variability of the dynamical system, provided the two following conditions.

First, the ensemble at the initial time must contain all

equally likely states. The initial PDF may be the PDF of the analysis error (Mullen and Baumhefner 1994), but in order to get the variability of the dynamical system, the PDF may instead represent its climatological error (Leith 1974). To have such a PDF representative of the dynamic system, a spectral selection is performed. It gives a high variability for the scales of the most unstable baroclinic modes, and the variability decreases at longer wavelengths away from the most unstable wavelength. The stability of the spectrum between the beginning and the end of the forecast was checked. In particular, the slope of the spectrum toward the high wavenumbers does not change, suggesting that the initial spectrum is coherent with the dynamic system. Moreover, in order to limit the numerical cost of this ensemble, the initial perturbations are located in a large circle of diameter 4000 km centered on the initial cyclone. This location is computed by multiplication with a bidimensional isotropic Gaussian-shaped function. Therefore, this initial sample is optimized so that it consists of all the perturbations that may interact with the cyclone with a reasonable numerical cost.

Second, the ensemble must be large enough. This is checked by looking at the final distribution and verifying that it does not change as the number of members in the ensemble increases. The convergence of the spread of vorticity at the final state has been tested, showing that a number of 2000 elements is sufficient. This result is consistent with the previous restrictions made on the useful wavelengths and locations, which limits the number of degrees of freedom ($\approx 10\,000$ for the model variable). Having computed this reference ensemble, it is now possible to assess other kinds of ensembles by comparison with the reference. Two diagnostics are performed for assessment.

First, the spread of vorticity σ_ζ at the final time is measured at every grid point. The points where the spread of one ensemble is high indicate the places where the elements of this ensemble take widespread values. Therefore, it can be understood as an indication of the different regions where the uncertainty in the scenarios is high. Figure 5 shows the spread of this reference ensemble in terms of vorticity at the surface (ground). As expected the highest spread is located along the sharpest gradient of vorticity associated with the main vortex (see Snyder et al. 2003). A secondary maximum exists in region \mathfrak{R} , which gives a sign but certainly not a proof of the existence of several scenarios in this region.

Second, histograms of the values of vorticity were computed for some relevant grid points. The information provided by the spread is incomplete and histo-

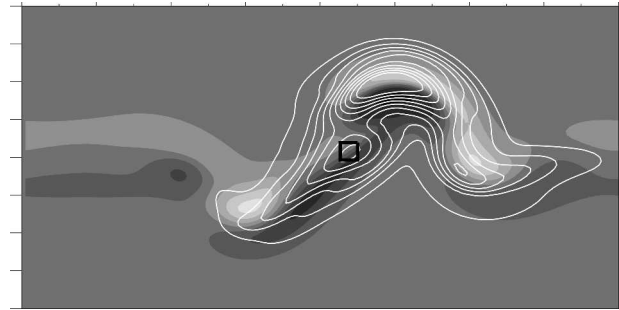


FIG. 5. Dispersion of the vorticity on the ground of the reference Monte Carlo ensemble (2000 elements) at time 96 h. The isolines of spread are white. The vorticity on the ground of the control simulation (Fig. 2) also appears in the background, with cyclonic regions darker and anticyclonic regions brighter. The black square is the region of nine grid points where the following histograms of vorticity are computed. Intervals of spread of vorticity: $3 \times 10^{-6} \text{ s}^{-1}$. Intervals of vorticity: $5 \times 10^{-6} \text{ s}^{-1}$.

grams are necessary to have a precise idea of the density of probability. The grid points selected are the ones highlighted in Fig. 5: a square of nine points centered on the relative maximum of spread of the Monte Carlo ensemble. The histogram shown in Fig. 6 reveals a bimodal behavior for the vorticity in this region. The distribution is fitted with the sum of two Gaussian PDFs using the least squares method (bi-Gaussian fit). The fit works actually quite well, and moreover, the two peaks

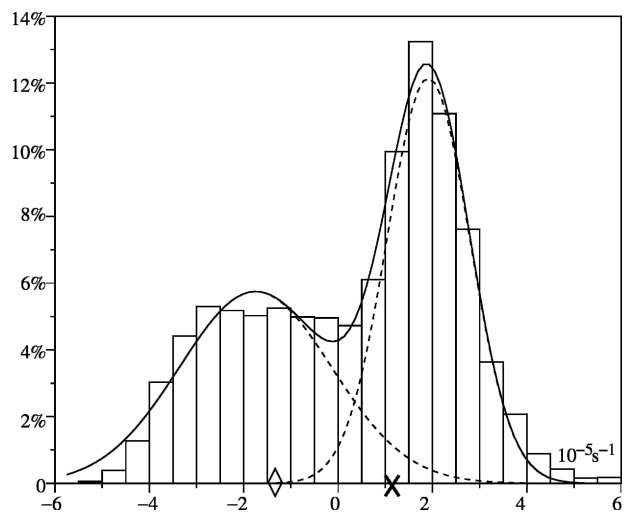


FIG. 6. Histogram of vorticity at the ground at the final time (96 h) for the reference Monte Carlo ensemble. Nine points (one central point + the eight nearest points) have been taken into account to build this histogram. The cross is the value of the control final state $11 \times 10^{-6} \text{ s}^{-1}$, and the diamond the value of the secondary state $-13 \times 10^{-6} \text{ s}^{-1}$ at the central point. The solid curve is the sum of two Gaussians that best fits the histogram in the least squares sense. The two Gaussians are also represented in dashed lines.

of the histogram are close to the values of relative vorticity for both scenarios. Therefore, both scenarios are indeed present in the variability of the dynamical system, and the Monte Carlo scheme expresses their natural probabilities given the initial error field. The parameters of the bimodal fit are recalled in Table 2.

c. Singular vectors

Three SV ensembles are calculated using different norms at initial and final time, but sharing the following features. The optimization time is 24 h, which is short enough to let the nonlinear processes work after optimization. At the initial time, the norm is computed over the entire domain as a uniform analysis error is assumed. At the optimization time, the norm is projected on an optimization window. It has an isotropic Gaussian shape centered at the same point as the main cyclone MV at 24 h. The radius of the window is typically 4000 km; it has been chosen by looking at the structure of the singular vectors for different sizes. The size of the window strongly constrains the envelope of the singular vectors. Since the jet stream is uniform and periodic, the first singular vectors without an optimization window are dominated by very large scales. They are also periodic, which is unrealistic. Therefore, an appropriate window helps to create useful perturbations for the cyclogenesis.

Two physical norms are defined: the Euclidian norm of the state vector ($\|\cdot\|^2 = \iint_{S^+} \theta^{+2} dS + \iint_{S^-} \theta^{-2} dS$) and the quasigeostrophic total energy norm ($\|\cdot\|^2 = \iiint_{S,z} \mathbf{u}_g^2/2 + (g/N)^2(\theta/\theta_0)^2 dS dz$). The Euclidian norm for the potential temperature state vector may also be seen as potential enstrophy (Bretherton 1966).

The initial norm may also be specified by the initial PDF. The reference Monte Carlo initial states are drawn from a known PDF whose variance-covariance matrix is named **C**. Ehrendorfer and Tribbia (1997) demonstrate that the singular vectors constrained initially by **C** account for the maximum part of variance at the optimization time. The most relevant comparison with the reference ensemble should use such singular vectors. Usually, an approximate of the analysis error is used to constrain the initial norm (e.g., Barkmeijer et

al. 1999). The appendix details the calculation of these singular vectors that use various norms at the initial and optimization time.

The three ensembles are a “regular” ensemble SV(r) (Euclidian norm, no initial constraint), an initially constrained with Euclidian norm singular vector ensemble SV(ice), and an initially constrained with total energy norm singular vector ensemble SV(ict). They all contain 20 members, which means that the first 10 singular vectors are calculated, then added or subtracted to the control initial state to generate 20 perturbations.

The constraint matrix **C** is diagonal in spectral space. There are no spectral correlations between different wavenumbers and between vertical levels. The only correlations in the Monte Carlo PDF are due to the initial spatial windowing of the perturbations. This feature is for numerical convenience and does not alter the comparison with the reference ensemble in region \mathfrak{R} .

Figure 7 represents the spread of vorticity of the singular vector ensembles at the final instant. The SV ensemble histograms corresponding to Fig. 6 are shown in Fig. 8. The spread map of SV(r) has the same pattern as the Monte Carlo reference, with maxima along the sharpest gradients of vorticity. But the intensity of the spread is lower. This singular vector ensemble underestimates the variability around the initial state. The histogram does not show a bimodal shape, but rather a Gaussian shape centered on the control simulation. Thus, the SV(r) ensemble does not reproduce the bimodal behavior that is expected. It creates some variance around the control run but does not make a secondary scenario appear.

The spread of SV(ice) covers a large zone compared to the Monte Carlo ensemble and SV(r). It is also less regular. The SV(ice) ensemble promotes larger scales than for the SV(r) ensemble; it produces perturbations that make the jet undulate on a large scale, whereas the optimization window plays a more important role for the SV(r) ensemble.

Besides, the initial covariance matrix does not take into account the limited location of the Monte Carlo ensemble. Thus the global spread map should be interpreted with care. Nevertheless, there is a local maxi-

TABLE 2. Features of the bimodal distribution.

	Reference	VP(l)	VP(s)	SV(r)	SV(ice)	SV(ict)	MC(s)
First peak (%)	12.2	13.6	14.3	—	10.8	8.7	11.3
First mean (10^{-5} s^{-1})	1.9	1.7	1.8	—	1.7	1.5	1.8
First spread (10^{-5} s^{-1})	0.8	0.6	0.5	—	1.2	1.6	0.8
Second peak (%)	5.8	8	8	—	4.6	8.4	9.23
Second mean (10^{-5} s^{-1})	-1.8	-1.4	-1.1	—	-2.2	-2.5	-1.66
Second spread (10^{-5} s^{-1})	1.6	1.4	1.8	—	1.2	0.7	1.24

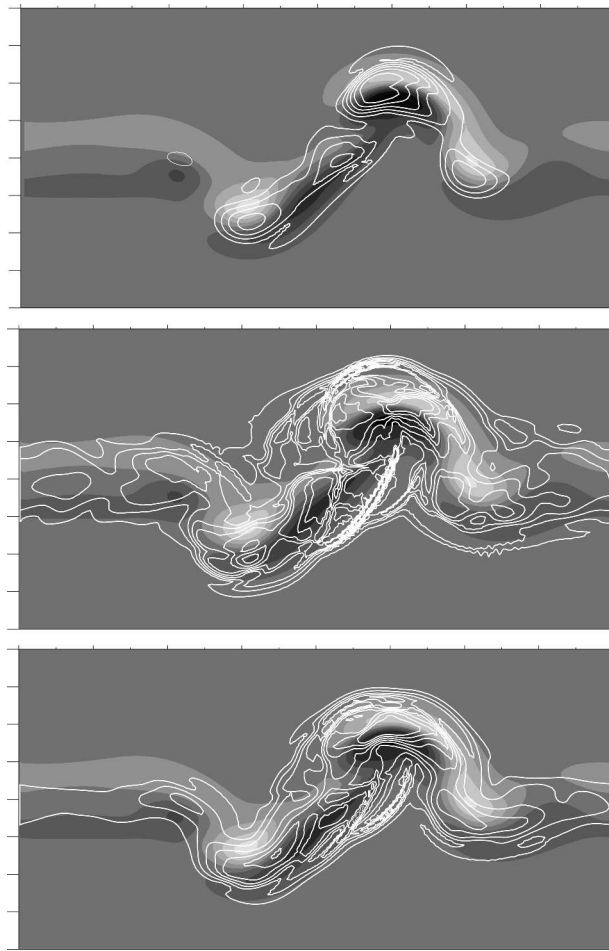


FIG. 7. Same as Fig. 5, but for the three singular vectors ensemble (20 elements each): (top) $SV(r)$, (middle) $SV(ice)$, and (bottom) $SV(ict)$.

mum of spread in region \mathcal{R} , and the histogram, which may be fitted by a bi-Gaussian, is close to the Monte Carlo histogram. This ensemble, which does not seem to be well designed for the local weak predictability (because of its large scales) captures the variability of the dynamical system in region \mathcal{R} .

The spread of $SV(ict)$ is more regular and is closer to the zones of gradient than $SV(ice)$. Classically, the total energy norm promotes smaller scales (Joly 1995). A maximum of spread appears in region \mathcal{R} , and the histogram shows a rather precise bimodal behavior although it is not close to the Monte Carlo histogram. For instance, the secondary scenario prevails too much in the variability of this ensemble. Several studies have shown the dependance of the singular vectors on the norm (Snyder and Joly 1998); it is therefore expected that the variability of a SV ensemble depends on the norm.

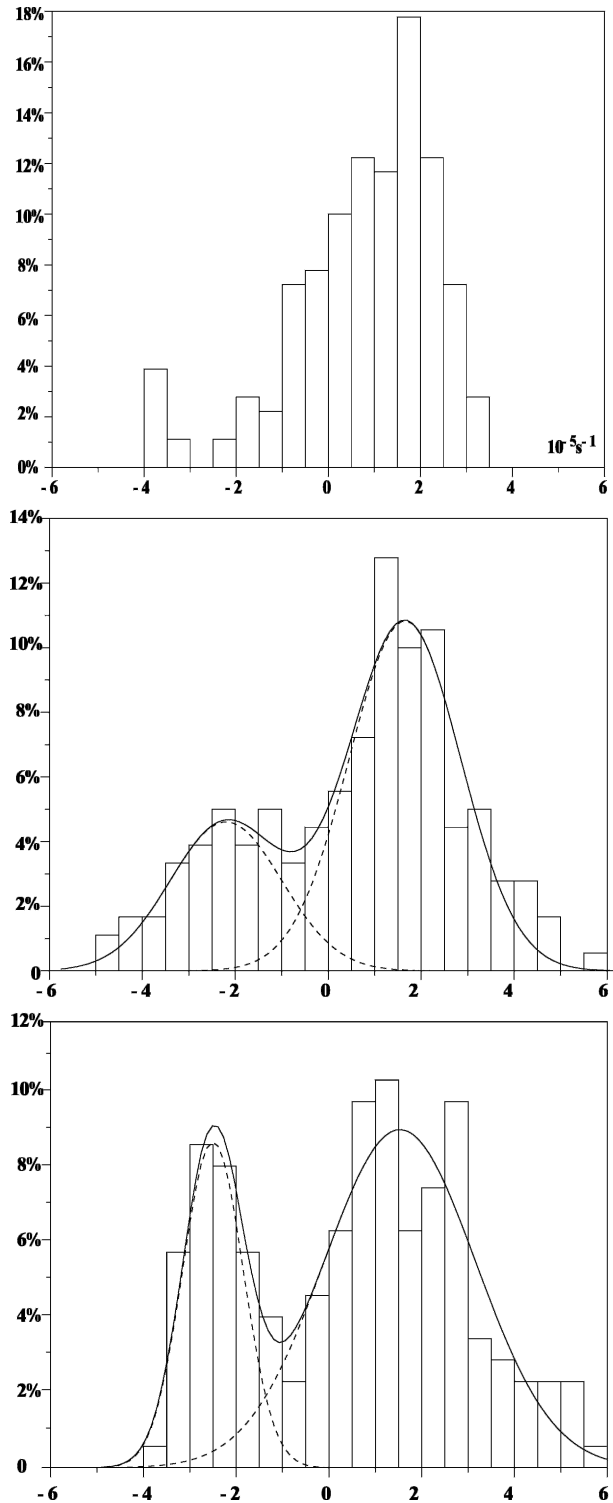


FIG. 8. Same as Fig. 6, but for the three singular vectors ensemble (20 elements each): (top) $SV(r)$, (middle) $SV(ice)$, and (bottom) $SV(ict)$.

d. Variation of the initial coherent structures

The initial state of an idealized cyclone is entirely controlled by 12 independent parameters that describe the shape, the amplitude, and the position of its precursors. By changing these parameters, a part of the phase space is explored and ensembles may be built. A preliminary survey helped to determine the parameters that have the largest impact on the forecast. Hence, five parameters were isolated: the vertical tilt, the amplitude of both anomalies, and their radius. An ensemble is built by sampling values for these five initial parameters. Then each perturbation is renormalized and the potential temperature spread of the ensemble equals the climatological analysis error, as described previously in the experimental framework.

A first large ensemble is considered: VP(l) (for variation of precursors, large). The five most important parameters vary on three modalities, thus creating an ensemble of $3^5 = 243$ members. The spread map (Fig. 9) of VP(l) follows the Monte Carlo reference, although remaining weaker. The histogram (Fig. 10) is very similar to the reference and shows two peaks for the same values as for the reference. It is thus possible to reproduce the variability of the dynamical system in region \mathfrak{R} with only 243 elements instead of 2000. This result validates the use of the VP method to assess the variability of this region. But this ensemble is still too large to be implemented operationally.

The SV and VP ensembles may be compared if the numerical cost of the computation of each ensemble is similar. To calculate an ensemble forecast on time range T with n members with optimization time $T/4$, one needs $2 \times 3 \times n/2 \times T/4 + n \times T$ (2 is for the tangent-linear run and its adjoint, $/2$ is because $n/2$ singular vectors are needed, and 3 is for the Lanczos algorithm). For the VP one needs $n \times T$ only. So the cost of SV is 75% higher for an optimization time quarter of the run time. Hence, to compare to the 20 members SV, 35 elements can be afforded. A small ensemble VP(s) is

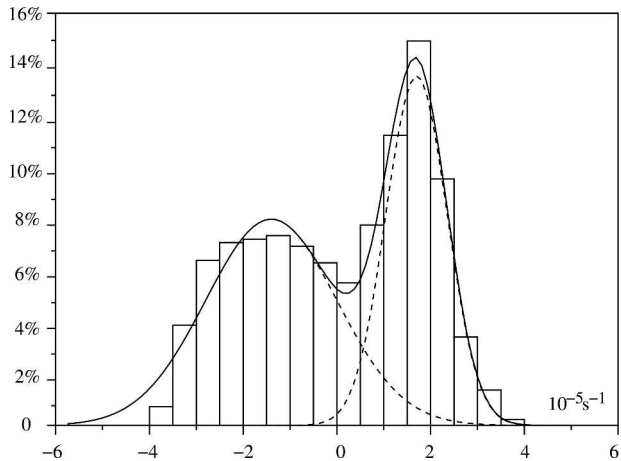


FIG. 10. Same as Fig. 6, but for the large variation of initial parameters ensemble VP(l).

set up with a number of members as close as possible to 35. The simplest solution is to have only three parameters vary among the five that were previously identified. The vertical tilt and the amplitude of both anomalies were chosen. Since baroclinic interaction is responsible for the weak predictability of the flow, they have a wider impact than the radius of the anomalies. Thus the VP(s) ensemble is smaller than what is allowed: it contains $3^3 = 27$ elements.

For the VP(s) ensemble, the spread map (Fig. 11) is similar to the one of VP(l) except for the anticyclonic structure that is located downstream of the main cyclone: it is still high along the sharpest gradients of vorticity although the intensity is weaker. The histogram (Fig. 12) has a similar shape, although the secondary peak does not emerge as well as in VP(l). VP(s) is then compared with the three SV ensembles. The intensity of the spread map is higher for the VP(s) than for SV(r) and it is closer to the reference than SV(ice) and SV(ict). The bimodal behavior of VP(s) is quite similar to the histogram of SV(ice), regarding both the

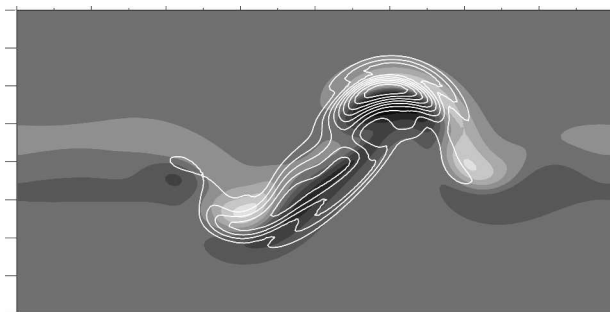


FIG. 9. Same as Fig. 5, but for the large variation of initial parameters ensemble [VP(l), 243 elements].

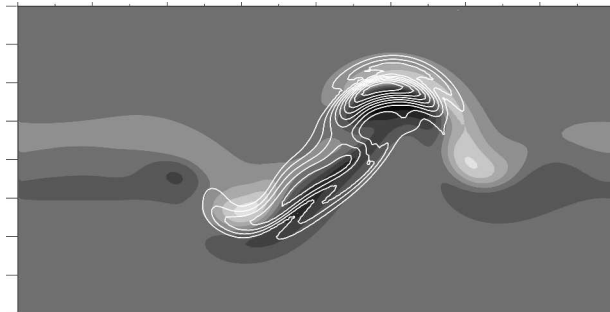


FIG. 11. Same as Fig. 5, but for the small variation of initial parameters ensemble [VP(s), 27 elements].

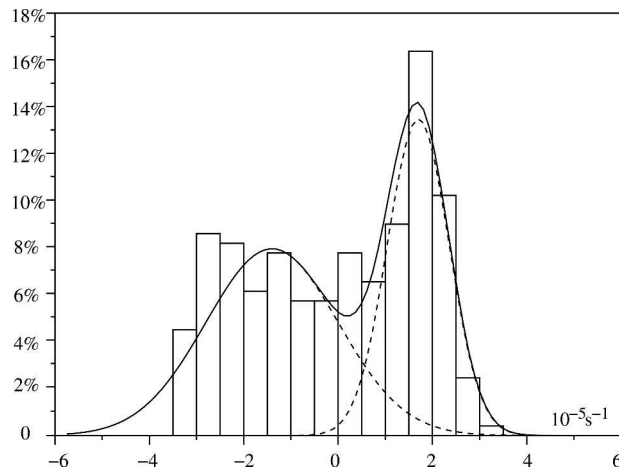


FIG. 12. Same as Fig. 6, but for the small variation of initial parameters ensemble VP(s).

quality of the fit and its features (Table 2). The VP and SV(ice) methods seem to be the most efficient for this short-term forecast.

e. A small Monte Carlo ensemble

A Monte Carlo ensemble whose computation requires the same cost as the singular vector ensembles is presented. The corresponding spread map and histogram are shown in Figs. 13 and 14. Although the convergence is not reached, this ensemble may be compared with the SV and VP ensembles. The spread map is very close to the reference, and the histogram shows a bimodal behavior. But the distribution overestimates the probability of the secondary scenario compared to the control.

5. Discussion about the error growth mechanism

The SV(r) ensemble fails to reproduce the bimodal PDF of the atmospheric state. Is this result linked to the fact that the error growth mechanism of the cyclogen-

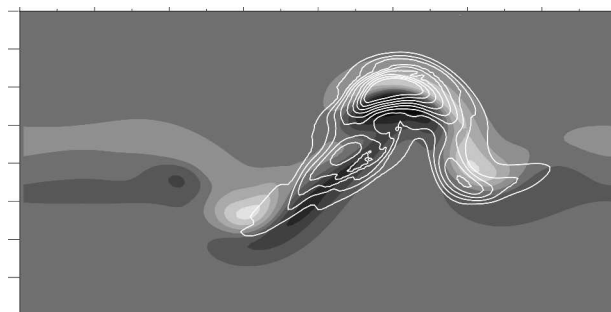


FIG. 13. Same as Fig. 5, but for the Monte Carlo ensemble of 35 members.

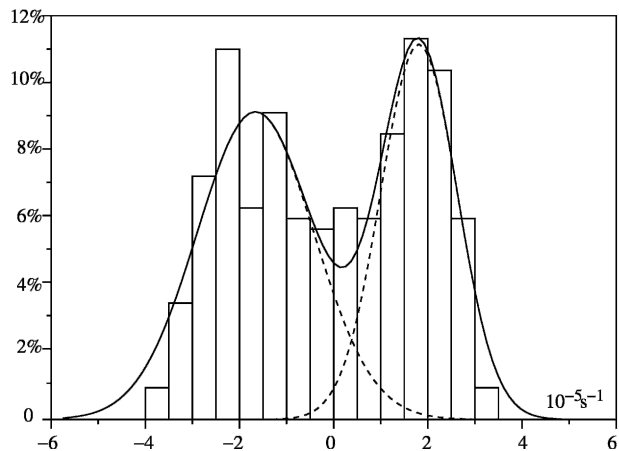


FIG. 14. Same as Fig. 6, but for the Monte Carlo ensemble of 35 members.

esis is nonlinear? The fact that the SV(ice) ensemble gives results similar to the VP ensemble helps to answer negatively to this question. Yet a further experiment was carried out to understand if there are dynamical reasons why the SV(r) ensemble is not efficient.

Starting from the control and secondary scenario initial states \mathbf{X}_0 and \mathbf{X}'_0 the coherent-structure-based initial perturbation is defined as $\mathbf{X}'_0 - \mathbf{X}_0$. It may be seen as a theoretical initial error on the position of coherent structures. This perturbation is projected on the subspace spanned by the first 10 singular vectors $\mathbf{SV}1, \dots, \mathbf{SV}10$ (orthonormal). Results show that

$$\begin{aligned} (\mathbf{X}'_0 - \mathbf{X}_0) / \|\mathbf{X}'_0 - \mathbf{X}_0\| = & 0.11\mathbf{SV}1 + 0.28\mathbf{SV}2 - 0.63\mathbf{SV}3 \\ & + 0.09\mathbf{SV}4 + 0.05\mathbf{SV}5 \\ & + 0.18\mathbf{SV}6 + 0.04\mathbf{SV}7 \\ & + 0.01\mathbf{SV}8 - 0.04\mathbf{SV}9 \\ & - 0.03\mathbf{SV}10 + \mathbf{SV}_\perp, \end{aligned}$$

where \mathbf{SV}_\perp is a residual orthogonal to the 10 SVs.

$\mathbf{SV}3$ has a quite strong negative correlation with $\mathbf{X}'_0 - \mathbf{X}_0$, and it should be interesting to examine the linear and nonlinear propagation of the initial perturbation $-\alpha\mathbf{SV}3$, α being a positive scalar such that the initial maximum in potential temperature is the same for $-\alpha\mathbf{SV}3$ as for $\mathbf{X}'_0 - \mathbf{X}_0$. The linear evolution uses the tangent-linear model of the control scenario. Figure 15 shows the relative vorticity at the surface for the nonlinear evolution of $\mathbf{X}_0 - \alpha\mathbf{SV}3$: the secondary scenario is well reproduced, with the existence of the anticyclonic vortex Ac (cf. with Fig. 2). The linear integration gives a relative vorticity map that is neither close to the secondary scenario nor to the control scenario. Figure 16 shows the maximum discrepancy in potential tem-

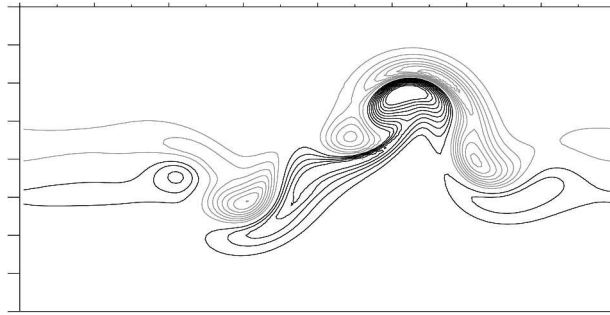


FIG. 15. Relative vorticity at the ground level at time 96 h for the evolution of $\mathbf{X}_0 - \alpha\mathbf{SV3}$. Same legend as Fig. 2.

perature between any simulation (secondary scenario, nonlinear, and linear evolution of $-\alpha\mathbf{SV3}$). The maximum discrepancy is equivalent to the L^∞ distance (Buizza and Palmer 1998) between two states, and this norm is more adapted to the local differences that are found during cyclogenesis. The error increases the most rapidly with the linear evolution of the singular vector. The nonlinearities of the dynamics slow the growth for the nonlinear evolution after 40 h; however it is still higher than for the error in initial position of coherent structures.

This experiment shows that at least one singular vector of $\mathbf{SV}(r)$ is able to reproduce an error growth mechanism due to the initial error of position of coherent structures. It is important to let the singular vector evolve nonlinearly, which requires that the optimization time should be short enough. The initial phase of error growth is slow enough to allow the assumption of small error and the validity of the tangent-linear model. Then the singular vectors evolve nonlinearly and they

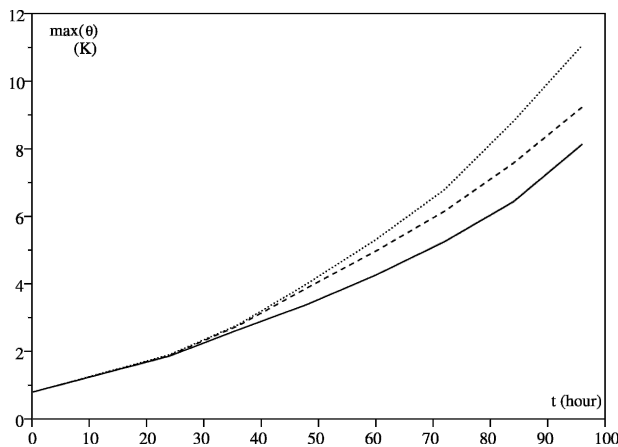


FIG. 16. Evolution of the maximum of difference of potential temperature between the control simulation and the three perturbations: coherent structures (solid line), nonlinear evolution of the SV (dashed line), and linear evolution of the SV (dotted line).

may reproduce the dynamics associated with the error on coherent structures. Indeed, the spread associated with one of them may be higher than for coherent structure (Fig. 16).

This result raises the question of why the singular vector ensemble $\mathbf{SV}(r)$ does not reproduce the variability of the dynamical system whereas the $\mathbf{SV}(\text{ice})$ does. The main difference between these two ensembles is that the $\mathbf{SV}(\text{ice})$ singular vectors are constrained by the PDF of the initial state. Thus it seems important to compute singular vectors that span optimally the initial PDF.

6. Conclusions

This study shows a quasigeostrophic flow for which two distinct scenarios of evolution are possible. A physical explanation of these separate developments is based on the baroclinic interaction between upper-level and lower-level coherent structures. A reference Monte Carlo ensemble is computed around the control simulation; then several other kinds of ensemble prediction systems are assessed. The main conclusions are drawn here.

- The existence of both scenarios appears in the variability of the dynamical system. The histogram of the Monte Carlo ensemble calculated at some relevant points has not a Gaussian shape but rather a bimodal shape.
- A large ensemble based on modifications of the initial coherent structures gives a bimodal distribution that is close to the reference. The variation of the precursors of the cyclone represents also the variability of the dynamical system, but this ensemble is too large for operational use.
- Three ensembles with size compatible with operational settings capture the bimodality of the scenario: a small Monte Carlo ensemble, a singular vector ensemble initially constrained by the initial PDF, and a small ensemble based on the modification of the precursors.
- The ensemble of singular vectors without initial constraint does not reproduce the two scenarios. This failure is not linked to the nonlinearity of the error growth mechanism, but rather to the fact that the ensemble does not span optimally the initial PDF.

The low-predictability case that is presented is similar to the ones described by Snyder (1999) in the sense that the main error growth mechanism is the effect of the interaction of coherent structures. Such a nonlinear error growth mechanism does not discard automatically singular vectors for an ensemble forecast provided they

evolve nonlinearly and they are adapted to the dynamics.

According to the results of this idealized study, the initial PDF has a crucial importance in order to obtain the variability of the atmosphere in a short-term forecast. In a perfect-model framework, this PDF is representative of the dynamics and it may be accessible through the initial coherent structures. A practical sampling of the initial PDF can be obtained through the variation of the precursors. This paper shows that such an ensemble samples the variability of some features of the cyclogenesis. This technique deserves further investigation.

Two new paths for future research in the initialization of short-term ensemble forecasting may be seen. The first technique could consist in extracting the coherent structures from a given analysis and modifying their features: shape, amplitude, and position. The resultant reinforcement, weakening, or loss of interaction between the precursors for each simulation of the ensemble may reproduce the variability of the dynamical system. The second method would define singular vectors constrained by these precursors. Both techniques would require one to identify the anomalies of operational fields using algorithms similar to the one used for potential vorticity by Demirtas and Thorpe (1999), or others.

In an operational system, one has to deal with the analysis error in addition. The analysis error emerges also where there are strong gradients; therefore it may be expected around the coherent structures. Thus both “coherent structures” methods would account for a part of the analysis error. Besides, the good results of multianalyses schemes (Richardson 2001) regarding their small size may be seen as a sign of the importance of the precursors. Indeed, a multianalyses scheme samples the initial PDF and modifies the features of coherent structures. The coherent structure concept is implicit in existing analysis and prediction systems, and making it more explicit could be a way to make further proposals. The issue of local predictability and short-term ensemble forecasting is still open and should receive focus in meteorological operational systems in the future.

Acknowledgments. The authors are deeply grateful to G. Hello for actively taking part in the initial phase of this work, and to J. Nicolau for providing ideas and technical material on the current short-term Ensemble Prediction System at Météo-France. The constructive comments of C. Snyder and two anonymous reviewers on the first version of the manuscript are gratefully acknowledged. The permanent guidance of A. Joly on this work is also sincerely acknowledged.

APPENDIX

Computation of the Singular Vectors

Let \mathbf{S} be the matrix of the scalar product, \mathbf{R}_t the tangent-linear propagator between time 0 and time t , \mathbf{P} , the projection operator on the optimization window, and \mathbf{C} the variance–covariance of the initial PDF. The singular vectors are the vectors \mathbf{v} that maximize the scalar product

$$\langle \mathbf{P}\mathbf{R}_t\mathbf{v}, \mathbf{P}\mathbf{R}_t\mathbf{v} \rangle_{\mathbf{S}}$$

subject to the constraint $\langle \mathbf{v}, \mathbf{C}^{-1}\mathbf{v} \rangle_{\mathbf{S}} = 1$ [which is a generalization to the non-Euclidian scalar products of Ehrendorfer and Tribbia 1997)]. This problem is equivalent to find the eigenpairs (\mathbf{v}, λ) that solve

$$\mathbf{R}_t^* \mathbf{P}^* \mathbf{S} \mathbf{P} \mathbf{R}_t \mathbf{v} = \lambda \mathbf{C}^{-1} \mathbf{S} \mathbf{v},$$

where $*$ denotes the Hermitian operator. The numerical solution is the Lanczos algorithm if $\mathbf{S} = \mathbf{C} = 1$ or the Jacobi–Davidson algorithm (Sleijpen and Van Der Vorst 1996) if $\mathbf{C}^{-1} \mathbf{S}$ is self-adjoint. The latter condition requires that \mathbf{C} and \mathbf{S} commute, and it is not easy to fulfill. However, in the context of the paper, \mathbf{C} is a diagonal matrix and \mathbf{S} is either 1 (Euclidian norm) or constituted by four square blocks that are diagonal (quasigeostrophic total energy norm), as written by Joly (1995). In any case, the matrices commute and the singular vectors may be computed.

REFERENCES

- Arbogast, P., 2004: Frontal wave development by interaction between a front and a cyclone: Application to the FASTEX IOP 17. *Quart. J. Roy. Meteor. Soc.*, **130**, 1675–1696.
- Barkmeijer, J., R. Buizza, and T. N. Palmer, 1999: 3D-var Hessian singular vectors and their potential use in the ECMWF Ensemble Prediction System. *Quart. J. Roy. Meteor. Soc.*, **125**, 2333–2351.
- Bretherton, F. P., 1966: Critical layer instability in baroclinic flows. *Quart. J. Roy. Meteor. Soc.*, **92**, 325–334.
- Buizza, R., and T. Palmer, 1998: Impact of ensemble size on ensemble prediction. *Mon. Wea. Rev.*, **126**, 2503–2518.
- Davies, H. C., C. Schär, and H. Wernli, 1991: The palette of fronts and cyclones within a baroclinic wave development. *J. Atmos. Sci.*, **48**, 1666–1689.
- Demirtas, M., and A. J. Thorpe, 1999: Sensitivity of short-range weather forecasts to local potential vorticity modifications. *Mon. Wea. Rev.*, **127**, 922–939.
- Ehrendorfer, M., and J. Tribbia, 1997: Optimal prediction of forecast error covariances through singular vectors. *J. Atmos. Sci.*, **54**, 286–313.
- Emanuel, K. A., M. Fantini, and A. J. Thorpe, 1987: Baroclinic instability in an environment of small stability to slantwise moist convection. Part I: Two-dimensional models. *J. Atmos. Sci.*, **44**, 1559–1573.
- Hamill, T. M., C. Snyder, and R. E. Morss, 2000: A comparison of

- probabilistic forecasts from bred, singular-vector, and perturbed observation ensembles. *Mon. Wea. Rev.*, **128**, 1835–1851.
- Hello, G., and P. Arbogast, 2004: Two different methods to correct the initial conditions, potential vorticity modifications and perturbations with sensitivities: An application to the 27 December storm over south of France. *Meteor. Appl.*, **11**, 1–17.
- Hoskins, B. J., and F. P. Bretherton, 1972: Atmospheric frontogenesis models: Mathematical formulation and solution. *J. Atmos. Sci.*, **29**, 11–37.
- , and P. Berrisford, 1988: A potential vorticity perspective of the storm of 15–16 October 1987. *Weather*, **43**, 122–129.
- Joly, A., 1995: The stability of steady fronts and the adjoint method: Non-modal frontal waves. *J. Atmos. Sci.*, **52**, 3082–3108.
- Leith, C. E., 1974: Theoretical skills of Monte Carlo forecasts. *Tellus*, **38A**, 97–110.
- Lorenz, E. N., 1963: Deterministic nonperiodic flow. *J. Atmos. Sci.*, **20**, 130–141.
- Molteni, F., R. Buizza, T. N. Palmer, and T. Petroliaigis, 1996: The ECMWF Ensemble Prediction System: Methodology and validation. *Quart. J. Roy. Meteor. Soc.*, **122**, 73–119.
- Mullen, S. L., and D. P. Baumhefner, 1994: Monte Carlo simulations of explosive cyclogenesis. *Mon. Wea. Rev.*, **122**, 1548–1567.
- Richardson, D., 2001: Ensembles using multiple models and analyses. *Quart. J. Roy. Meteor. Soc.*, **127**, 1847–1864.
- Schär, C., and H. Wernli, 1993: Structure and evolution of an isolated semi-geostrophic cyclone. *Quart. J. Roy. Meteor. Soc.*, **119**, 57–90.
- Simmons, A. J., and B. J. Hoskins, 1978: The life cycles of some non-linear baroclinic waves. *J. Atmos. Sci.*, **35**, 414–432.
- Sleijpen, G. L. G., and H. A. Van Der Vorst, 1996: A Jacobi–Davidson iteration method for linear eigenvalue problems. *SIAM J. Matrix Anal. Appl.*, **17**, 401–425.
- Snyder, C., 1999: Error growth in flows with finite-amplitude waves or other coherent structures. *J. Atmos. Sci.*, **56**, 500–506.
- , and A. Joly, 1998: Development of perturbations within growing baroclinic waves. *Quart. J. Roy. Meteor. Soc.*, **124**, 1961–1983.
- , T. M. Hamill, and S. B. Trier, 2003: Linear evolution of error covariances in a quasigeostrophic model. *Mon. Wea. Rev.*, **131**, 189–205.
- Takayabu, I., 1991: Coupling development: An efficient mechanism for the development of extratropical cyclones. *J. Meteor. Soc. Japan*, **69**, 609–628.
- Thorncroft, C. D., and B. J. Hoskins, 1990: Frontal cyclogenesis. *J. Atmos. Sci.*, **47**, 2317–2336.
- Toth, Z., and E. Kalnay, 1993: Ensemble forecasting at NMC: The generation of perturbations. *Bull. Amer. Meteor. Soc.*, **74**, 2317–2330.
- Ziehmann, C., 2000: Comparison of a single-model EPS with a multi-model ensemble consisting of a few operational models. *Tellus*, **52**, 280–299.